Modeling fluid transport in PEM fuel cells using the lattice-Boltzmann approach

L.-P. Wang & B. Afsharpoya
Department of Mechanical Engineering, University of Delaware, Newark, U.S.A.

Abstract

Three viscous flow problems relevant to fuel cell modeling are considered with the lattice Boltzmann approach. The first problem is a 3D viscous flow through a section of serpentine channel and the second is a 2D channel filled or partially filled with a porous medium. In the first case, attention is given to the implementation details such as inlet-outlet boundary conditions, nonuniform grid, and forcing. In the second case, the effects of multiple time scales and interface between the porous medium and clear channel are considered. In the third problem, these techniques are combined to simulate flow in a serpentine channel with GDL. Results are compared with other studies based on Navier-Stokes CFD and experimental observations.
Keywords: lattice Boltzmann approach, simulation, fuel cells, serpentine channel, porous medium, pressure loss.

1 Introduction

Fuel cells are electrochemical reactors generating electricity directly from oxidation reactions of fuels. Due to their high efficiency (typically twice of the energy conversion efficiency of internal combustion engines), near-zero emissions, low noise, and portability, fuel cells are being considered as a potentially viable energy-conversion device for mobile, stationary, and portable power. The low operation temperature of the proton-exchange membrane fuel cell (PEMFC) makes it a preferred fuel-cell type for automotive applications. A PEMFC unit consists of two thin, porous electrodes (an anode and a cathode) separated by a membrane-electrode assembly. Reactants (e.g., hydrogen and air) are brought into the cell through flow distribution channels (Fig. 1(a)). Computational models of increas-

WIT Transactions on Engineering Sciences, Vol 52, © 2006 WIT Press
www.witpress.com, ISSN 1743-3533 (on-line)
doi:10.2495/AFM06029

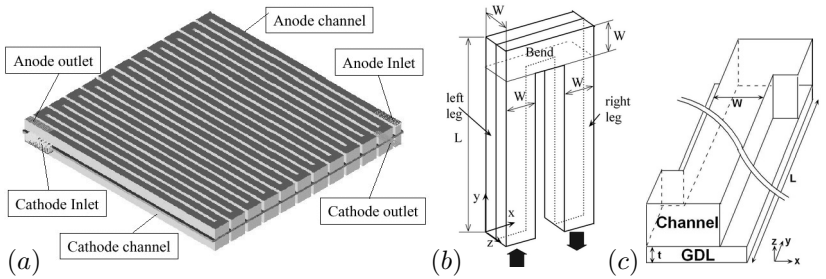

Figure 1: (a) Sketch of serpentine flow channels in PEM fuel cell; (b) A section of the channel being modeled in section 2; (c) A section of the channel with GDL being modeled in section 4.

ing complexity are currently being developed to better understand issues related to the performance of PEMFC, such as pressure loss and temperature distribution in the flow channels, species transport through porous gas diffusion layers (GDL), and water management on the cathode side. Wang [1] provides a review of recent modeling efforts using traditional computational fluid dynamics (CFD) based on macroscopic conservation equations.

In this paper we explore the use of lattice Boltzmann (LB) approach as a modeling tool for predicting fluid flows relevant to PEMFC. The LB approach is based on a kinetic formulation and could have certain advantages over the traditional CFD [2]. While LB models capable of addressing thermal flows, flows through porous media, multiphase flows, electro-osmotic flows, and contact line, *etc.*, have been proposed in recent years, two general aspects remain to be studied before they can be applied to fuel cell modeling. The first aspect concerns the accuracy and reliability of these models for practical applications. Since these models have typically only been tested for idealized problems, their applications to PEMFC flow problems need to be critically examined and different possible LB models be compared. The second aspect concerns a variety of implementation issues when dealing with practical applications, such as nonuniform grid, forcing implementation, boundary conditions, and porous-medium interface.

2 Flow through a serpentine channel without GDL

As a first example, we investigate the pressure distribution and flow pattern in a section of serpentine channel over a range of Reynolds numbers encountered in PEMFC. The channel has a square cross section of width W and a side length L (Fig. 1(b)). As a first step, we consider isothermal laminar flow and neglect the flow into the GDL so that the back wall is treated as a no-slip wall. This similar flow was studied recently by Matharudrayya *et al.* [3] using a traditional finite-volume CFD code and by Martin *et al.* [4] using particle imaging velocimetry (PIV).

The LB equation for the distribution function (DF) f_i of the particle with velocity $\mathbf{e}_i$

$$f_i(\mathbf{x}+\mathbf{e}_i\delta_t, t+\delta_t) - f_i(\mathbf{x},t) = -\frac{1}{\tau}\left[f_i(\mathbf{x},t) - f_i^{(eq)}(\mathbf{x},t)\right] + \psi_i(\mathbf{x},t) \quad (1)$$

is solved with a prescribed forcing field ψ_i designed to model the pressure difference between the inlet and the outlet, so that a periodic boundary condition can still be applied to f_i between the inlet and outlet. This minimizes the density fluctuations associated with f_i which could otherwise be significant considering the large L/W ratio here and the augmented pressure loss through the bend. The D3Q19 model is used with the following equilibrium distribution function

$$f_i^{(eq)}(\mathbf{x},t) = \omega_i\rho\left[1 + \frac{\mathbf{e}_i\cdot\mathbf{u}}{c_s^2} + \frac{\mathbf{uu}:(\mathbf{e}_i\mathbf{e}_i - c_s^2\mathbf{I})}{2c_s^4}\right], \quad (2)$$

where ω_i is the weight and the sound speed c_s is $1/\sqrt{3}$.

Two different methods of specifying the forcing term were tested. The first method specifies ψ_i and macroscopic variables as

$$\psi_i(\mathbf{x},t) = \omega_i\mathbf{e}_i\cdot\mathbf{F}/c_s^2,\ \rho = \sum_i f_i,\ \rho\mathbf{u} = \sum_i f_i\mathbf{e}_i,\ p = \rho c_s^2 + p_0(\mathbf{x}) \quad (3)$$

where ρ, $\mathbf{u}$, and p are the fluid density, velocity, and pressure, respectively. The macroscopic force field is defined as $\mathbf{F} = (0, A(1-y/L_1), 0)$ for the left leg of the channel and $\mathbf{F} = (0, -A(1-y/L_1), 0)$ for the right leg, with $L_1 = L - W$. In the bend region, $\mathbf{F} = 0$. This force field amounts to an auxiliary pressure field of $p_0(\mathbf{x}) = A(L_1-y)^2/(2L_1)$ in the left leg and $p_0(\mathbf{x}) = -A(L_1-y)^2/(2L_1)$ in the right leg and a total pressure difference of AL_1 between the inlet and outlet (the driving force for the flow). The coefficient A was set to $8\rho\nu v_0/W^2$, where the kinematic viscosity is related to the relaxation time as $\nu \equiv (\tau - 0.5)c_s^2\delta_t$ and v_0 is a velocity scale (of similar magnitude as the mean flow speed u_0). Guo *et al.* [5] showed that the forcing term in the above formulation introduces some lattice effects to the Navier-Stokes equation. They were able to remove the lattice effects by modifying the definitions of ψ_i and $\mathbf{u}$ [5]. For the current problem, we found, however, that the two methods gave almost identical results.

A nonuniform mesh along the $y-$direction (Fig. 1(b)) is necessary for computational efficiency. We have developed a Lagrangian interpolation method to compute DF at a grid point from the DFs on a shifted grid defined by the streaming step. The method generalizes the interpolation-supplemented LB method of He *et al.* [6] and is easier to implement than the Taylor series expansion and least squares-based LB method of Shu *et al.* [7]. The walls are located in the middle of lattice links so a second-order accuracy is achieved with a simple bounce-back algorithm.

Fig. 2 shows a typical pressure distribution along the centerline of the channel. If the channel is made very long ($L >> W$), the pressure should change linearly with distance away from the bend region at both the inlet and outlet, with a same

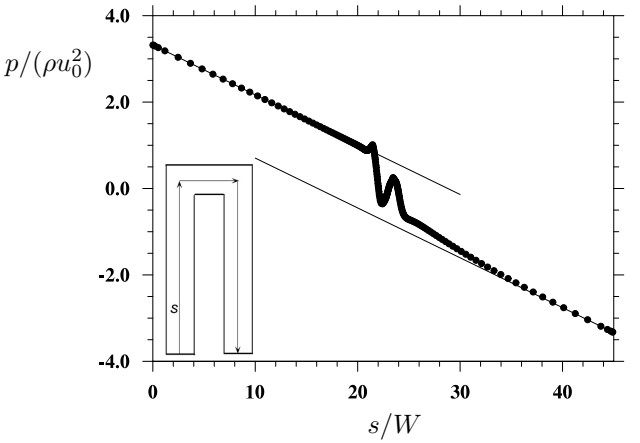

Figure 2: The pressure as a function of the distance s along the centerline of the channel when $Re = 127$.

slope. This slope away from the bend can be used to define a friction factor for a straight channel (i.e., $f = W\Delta p/(L\rho u_0^2/2)$) and the results are shown in Fig. 3(a) as a function of flow Reynolds number Re. This friction factor can be well modeled by the friction factor in a circular pipe (i.e., $f = 64/Re$) with diameter defined as $D = 2W/\sqrt{\pi}$, namely, diameter corresponding to same cross-sectional area. The deviation at large Re could be due to the influence of the bend since the value of L used ($L = 22W$) is not long enough.

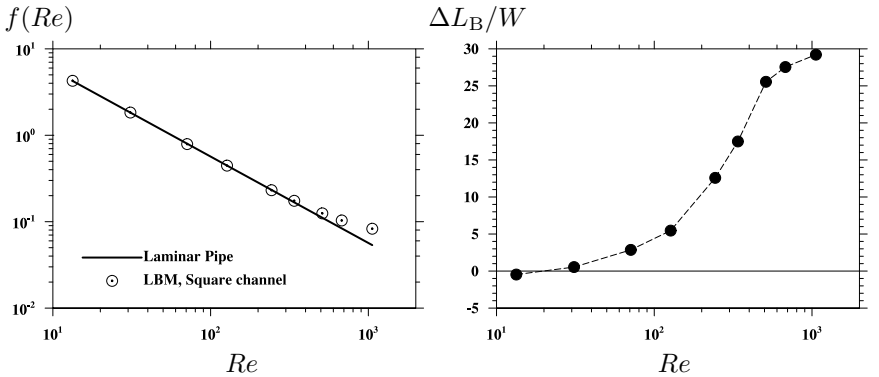

Figure 3: (a) The friction factor for the straight portion of the channel away from the bend. (b) The augmented loss due to the bend measured as the equivalent length of a straight channel.

A finite jump in pressure due to the bend exists, as indicated by the vertical distance between the two thin parallel lines in Fig. 2. This is referred to as the

bend pressure loss. The ratio of this jump to the slope away from the bend region defines a normalized, equivalent length for the bend pressure loss, $\Delta L_{\mathrm{B}}/W$. This equivalent length is shown in Fig. 3(b) as a function of Re. Of importance is that this length increases quickly with Re to values comparable to the actual single-path length in a typical PEMFC, implying that the bend pressure loss must be considered in fuel cell flow modeling. The slight negative value at the lowest Re is due to the fact that the flow can make 180-degree turn along the inner bend at such low Re.

Finally, we found that the flow in the bend region becomes unstable and small-scale vortices form at $Re \approx 1000$. To our knowledge, no accurate simulations for this Re range for a serpentine channel were made previously. Further analysis of this Re dependence will be reported in detail in a separate paper.

3 Flow through a channel filled or partially filled with porous medium

This section is motivated by the need to consider the interface between porous medium and flow channel in PEMFC modeling. We first consider flow in a 2D channel filled with porous medium of given porosity ϵ and permeability K. The macroscopic variables averaged over a representative elementary volume (REV) [8, 9] are considered and they are governed by the following momentum equation incorporating a Brinkman-extended Darcy law

$$\begin{gathered}\frac{\partial \mathbf{u}}{\partial t} + (\mathbf{u}\cdot\nabla)\left(\frac{\mathbf{u}}{\epsilon}\right) = -\frac{1}{\rho}\nabla(\epsilon p) + \nu_e\nabla^2\mathbf{u} + \mathbf{F} \\ \text{with } \mathbf{F} = -\frac{\epsilon\nu}{K}\mathbf{u} - \frac{\epsilon F_\epsilon}{\sqrt{K}}|\mathbf{u}|\mathbf{u} + \epsilon\mathbf{G},\end{gathered} \tag{4}$$

where the REV-averaged velocity $\mathbf{u}$ is assumed to be divergence-free, ν is fluid viscosity, ν_e is an effective viscosity, G represents the driving force for the flow. The geometric factor F_ϵ depends on the porosity and the microscopic configuration of porous medium (for details, see [8, 9]). This approach recovers the usual Navier-Stokes equation if $\epsilon \to 1$.

An LB model for the above macroscopic partial differential equation has been rigorously derived by Guo and Zhao [9]. The LB equation is identical to Eq. (1), but with f_i^{eq} and ψ_i modified as

$$f_i^{(eq)} = \omega_i\rho\left[1 + \frac{\mathbf{e}_i\cdot\mathbf{u}}{c_s^2} + \frac{\mathbf{uu}:(\mathbf{e}_i\mathbf{e}_i - c_s^2\mathbf{I})}{2\epsilon c_s^4}\right], \tag{5}$$

$$\psi_i = \omega_i\left(1 - \frac{1}{2\tau}\right)\left[\frac{\mathbf{e}_i\cdot\mathbf{F}}{c_s^2} + \frac{\mathbf{uF}:(\mathbf{e}_i\mathbf{e}_i - c_s^2\mathbf{I})}{\epsilon c_s^4}\right]. \tag{6}$$

We first apply the above model to a 2D channel of width H filled with porous medium. The flow is initially at rest and is driven by a constant pressure gradient G along the flow direction. In this case, the unidirectional transient flow subjected

to the boundary conditions $u(y=0,t)=u(y=H,t)=0$ can be solved analytically, giving

$$u(y,t)=\frac{GK}{\nu}\left\{1-\frac{\cosh[r(y-0.5H)]}{\cosh[0.5rH]}\right\}-\sum_{k=1,3,5,\ldots}^{\infty}\frac{4GK}{\nu}\frac{(\pi k)^2}{(\pi k)^2+(rH)^2}$$
$$\times\sin\frac{\pi ky}{H}\exp\left\{-\left[(\pi k)^2+(rH)^2\right]\frac{\nu_e t}{H^2}\right\}, \qquad (7)$$

where $r\equiv\sqrt{\nu\epsilon/(\nu_e K)}$. The analytical solution implies that there are two time scales in this problem, a diffusion time scale due to the channel walls $T_1\equiv H^2/(\pi^2\nu_e)$ and a diffusion time scale within the porous medium $T_2\equiv K/(\epsilon\nu)$. The ratio of the two time scales T_2/T_1 is equal to $\pi^2 Da/\epsilon$, which can be very small if the permeability is small. Here the Darcy number is defined as K/H^2. We find that in the implementation of the above LB scheme, it is necessary to use a very small Darcy velocity or a large H to ensure that both T_1 and T_2 are such larger than one. Otherwise, an apparent slip may be present near the walls, regardless whether the midway bounce-back or the nonequilibrium extrapolation method [10] was used on the walls. This slip disappears and the analytical solution can be precisely recovered when $T_1>>1$ and $T_2>>1$. A permissible lower bound for the time scales is found to be about 50 lattice time units.

We then simulated flow in a channel partially filled with porous medium so there is an interface inside the channel. The velocity varies continuously across the interface only when a very small Dracy velocity was used, for the reason indicated above. Two different treatments near the interface were tested. The first method places the interface in between the lattice nodes so that only the streaming step lead to exchanges of DF between two sides of the interface. The second method treats the interface as a boundary using the nonequilibrium extrapolation method, with the density and velocity taken as the average value from the two neighboring lattice points on the two sides of the interface. The results from the two treatments are almost identical. The results are also compared with the experimental data of Gupte and Advani [11]. The discrepancy in the clear channel region near the interface may be caused by the fact that the interface is not sharply defined in the experiment. Further investigation is underway to understand the origin of this discrepancy.

4 Flow through a serpentine channel with GDL

In this section, we combine the LB models discussed above to simulate fluid flow through a serpentine channel with GDL. A similar flow problem was recently studied by Pharoah [12] using a commercial, Navier-Stokes package (i.e., Fluent). Experimental measurements of fluid flow with the similar setting were performed by Feser [13].

For computational efficiency, a minimum periodic domain (see Fig 1(c)) with $0\le x\le 2W, 0\le y\le L, 0\le z\le (t+W)$ was considered, following the

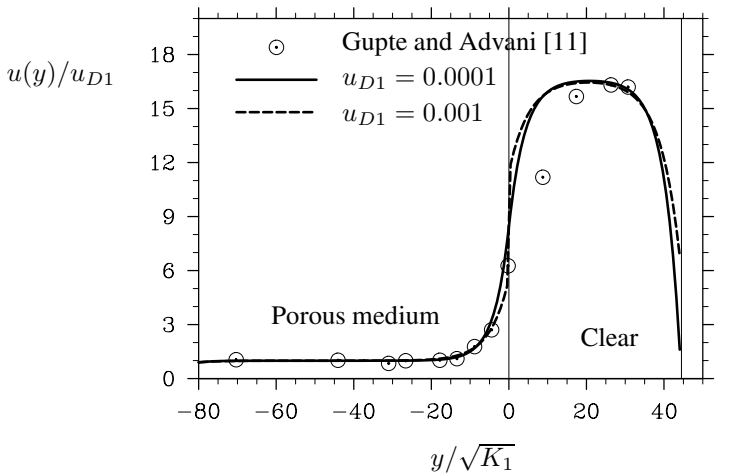

Figure 4: Velocity profile in a channel partially filled with porous medium. Parameters are: $\epsilon = 0.07$, $Re = 0.107$, $K_c/K_1 = 16.634$, and $Da = 5.611e-5$. Only a part of the channel is shown. The interface is located at $y = 0$.

analytical work of Feser [13]. Here L is the total length of the fuel cell, W is the width of the square flow channel, and t is the height of the GDL. The domain covers half of a complete serpentine loop. The inlet section at $x = 0$ consists of the cross section of the channel and the full section of GDL layer at the middle of a bend. The outlet is a cut through the middle of the immediate, opposite bend. The periodic boundary condition is

$$\mathbf{u}(0, y, z) = \mathbf{u}(2W, L - y, z), \quad \text{for } 0 \leq y \leq L \text{ and } 0 \leq z \leq (t + W). \tag{8}$$

In our simulations, we assumed that $L/W = 38$, $t/W = 1/3$, and W is 36 lattice units. A constant forcing per unit fluid mass of magnitude $F_0 = 8u_0\nu(L+W)/W^3$ is applied in the x direction to drive the flow in the LB equation. The forcing is added back when defining the macroscopic pressure field, namely, $p \equiv c_s^2 \sum f_i + \rho F_0(2W - x)$.

The results are compared with those of Pharoah [12] in Table 1. Note that Pharoah [12] used $L/W = 40$ and $t/W = 0.25$. The symbols in the table are: Re is the Reynolds number based on the total volumetric flow rate Q and W, Re_C is the Reynolds number based on the average velocity at the inlet channel and W, Re_{GDL} is the Reynolds number based on the average velocity at the GDL inlet and t, Q_C is the volumetric flow rate through the inlet channel only, and the pressure drop was normalized by $\rho(Q/W^2)^2$ or equivalently by $Re^2\rho(\nu/W)^2$. The air density and viscosity in Pharoah [12] are assumed to be 1 kg/m^3 and 0.17 cm^2/s, respectively. Several observations can be made: (1) the percentage of fluid flux through the channel decreases quickly with the Darcy number ($Da = K/W^2$)

Table 1: Flow partition and pressure drop in a serpentine channel with GDL.

	Re	Re_C	Re_{GDL}	Da	Q_C/Q	$\lvert\Delta\tilde{p}\rvert$
Run1	257.0	224.6	0.85	10^{-5}	87.4%	9.46
Run2	572.1	475.5	2.53	10^{-5}	83.2%	5.74
Run3	509.8	227.4	7.43	10^{-4}	44.6%	2.40
Run4	1624	268.1	35.7	10^{-3}	16.5%	0.24
Pharoah (2005)	200.0			10^{-5}	∼90%	~ 10.9
Pharoah (2005)	400.0			10^{-5}	∼87%	~ 6.81
Pharoah (2005)	400.0			10^{-4}	∼50%	~ 3.03
Pharoah (2005)	400.0			10^{-3}	∼22%	~ 0.54

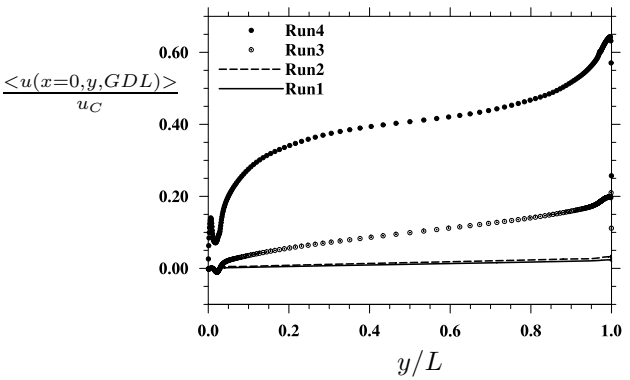

Figure 5: The z-averaged, x-component velocity through the middle of the GDL layer (i.e., x=0).

when $10^{-5} \leq Da \leq 10^{-3}$; (2) the percentage of fluid flux through the channel decreases slightly with flow Reynolds number, (3) both the pressure drop and the percentage of flow in channel agree reasonably well with the results of Pharoah [12], and finally (4) since our flow Reynolds number is higher, the percentage of flow in channel is lower than the values of Pharoah [12]. It is possible to match exactly the flow Reynolds numbers by adjusting the magnitude of u_0 appeared in the forcing F_0.

The vertically averaged, x-component velocity through the DGL at $x = 0$ is shown in Fig. 5 for the same four runs shown in table 1. In general, the velocity increases with y since the pressure difference on the two neighbouring channels above the GDL increases. At large Da, the flows through the channel and GDL are strongly coupled so that the convection velocity in GDL is strongly affected by the channel bends.

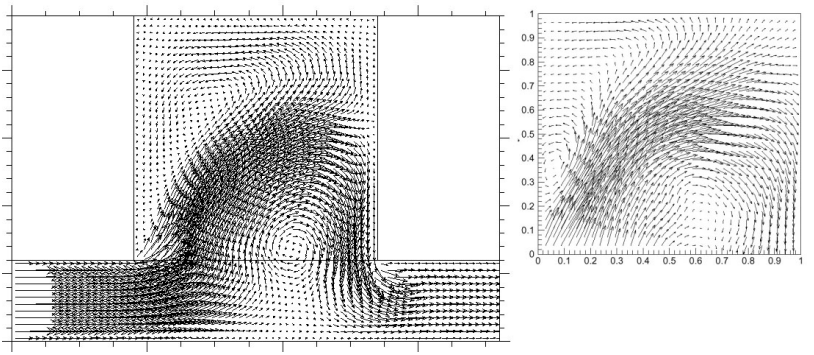

Figure 6: A snapshot of the quasi-steady velocity field in the $x - z$ plance, at a y location of one W before the exit bend. The left panel is from run4 and the right panel from PIV study of Feser [13].

Finally, the velocity field through an $x-z$ plane near the exit bend ($y = L-2W$) is compared with the PIV results of Feser [13]. The velocity is normalized by the average velocity u_C through the channel inlet. A strong convection flow through GDL generates secondary flows in the channel. This secondary flow differs from the self-generated secondary flow due to channel bends.

5 Conclusions

Three flow problems relevant to PEMFC are simulated with the LB approach. A 3D viscous flow through a section of serpentine channel without GDL was simulated and shown to depend sensitively on the flow Reynolds number. The pressure distribution along both the straight portion and bend region of the channel can be quantitatively modeled. We also demonstrate that flow through a porous medium with an interface can be treated with the LB approach, provided that the existence of multiple macroscopic time scales is taken into consideration. Finally, 3D flows through a serpentine channel with GDL were considered and it is shown that results on pressure drop and flow convection through GDL agree well with other Navier-Stokes CFD and PIV results.

Acknowledgements

This study is supported by the U.S. Department of Energy. The authors thank Professors Advani and Prasad of the University of Delaware for helpful discussions.

References

[1] Wang, C.Y., Fundamental models for fuel cell engineering. *Chem. Rev.* **104**, pp.4727-4766, 2004.

[2] Chen, S. and Doolen, G.D., Lattice Boltzmann method for fluid flows, *Annu. Rev. Fluid Mech.* **30**, 329-364, 1998.
[3] Maharudrayya, S., Jayanti S., & Deshpande, A.D., pressure losses in laminar flow through serpentine channels in fuel cell stacks. *J. Power Sources* **138**, pp.1-13, 2004.
[4] Martin, J., Oshaki, P., & Djilali, N., Flow structures in a u-shaped fuel cell flow channel: quantitative visualization using particle imaging velocimetry. *J. Fuel Cell Sci. Technol.*, in press.
[5] Guo, Z.L., Zheng, C.G., and Shi, B.C., Discrete lattice effects on the forcing term in the lattice Boltzmann method. *Phys. Rev. E.* **65**, 046308, 2002.
[6] He, X., Luo, L.-S., & Dembo, M., Some progress in lattice Boltzmann method. Part I. Nonuniform mesh grids. *J. Comp. Phys.* **129**, pp.357-363, 1996.
[7] Shu, C., Niu, X.D., & Chew, Y.T., Taylor series expansion and least squares-based lattice Boltzmann method: Three-dimensional formulation and its applications. *Int. J. Modern Physics C* **14**, pp.925-944, 2003.
[8] P. Nithiarasu, K.N. Seetharamu, and T. Sundararajan, Natural convective heat transfer in a fluid saturated variable porosity medium. *Int. J. Heat Mass Transfer* **40**, pp.3955-3967, 1997.
[9] Guo, Z.L. & Zhao, T.S., Lattice Boltzmann model for incompressible flows through porous media. *Phys. Rev. E.* **66**, 036304, 2002.
[10] Guo, Z.L., Zheng, C.G., and Shi, B.C., Non-equilibrium extrapolation method for velocity and pressure boundary conditions in the lattice Boltzmann method. *Chinese Phys.* **11**, pp.366-374, 2002.
[11] Gupte, S. & Advani, S.G., Non-Darcy flow near the permeable boundary of a porous medium: An experimental investigation using LDA. *Exp. in Fluids* **22**, pp.408-422, 1997.
[12] Pharoah, J.G., On the permeability of gas diffusion media used in PEM fuel cells. *J. Power Sources*, **144**, pp.77-82, 2005.
[13] Feser, J. Convective Flow Through Polymer Electrolyte Fuel Cells. M.S. thesis, University of Delaware, Newark, Delaware, USA, 2005.